WT-1103

Copy No. 218 A

Operation TEAPOT

NEVADA TEST SITE

February – May 1955

34 p

Project 1.3

GROUND-LEVEL MICROBAROGRAPHIC PRESSURE MEASUREMENTS FROM A HIGH-ALTITUDE SHOT

HEADQUARTERS FIELD COMMAND, ARMED FORCES SPECIAL WEAPONS PROJECT
SANDIA BASE, ALBUQUERQUE, NEW MEXICO

[redacted]

[redacted]

WT-1103

UNCLASSIFIED

This document consists of 36 pages
No. 218 of 220 copies, Series A

Report to the Test Director

GROUND-LEVEL MICROBAROGRAPHIC PRESSURE MEASUREMENTS FROM A HIGH-ALTITUDE SHOT

By

J. W. Reed
J. R. Banister
F. H. Shelton

Sandia Corporation
Sandia Base
Albuquerque, New Mexico

[redacted]

UNCLASSIFIED

ABSTRACT

Time records of incident and reflected overpressures from the high-altitude burst (Shot 10) of Operation Teapot were obtained at an array of ground stations. Modified Sachs' scaling to sea level for 1 kt gives overpressure results in agreement with an extension of the pressure-distance curve determined from canister data. Acoustic refraction did not appreciably alter the pressure-distance effects on this occasion. Shock-wave time parameters for this test were found to satisfy ordinary Sachs' scaling. An average pressure reflection factor of 0.92 was observed, but no correlation with surface parameters was obtained.

FOREWORD

This is one of the reports presenting the results of the 47 projects participating in the Military Effects Tests Program of Operation Teapot, which included 14 test detonations. For readers interested in other pertinent test information, reference is made to WT-1153, Summary Report of the Technical Director, Military Effects Program. This summary report includes the following information of possible general interest.

1. An over-all description of each detonation, including yield, height of burst, Ground Zero location, time of detonation, ambient atmospheric conditions at detonation, etc., for the 14 shots.
2. Discussion of all project results.
3. A summary of each project, including objectives and results.
4. A complete listing of all reports covering the Military Effects Tests Program.

ACKNOWLEDGMENTS

Particular gratitude is expressed to Charles Hoover and other personnel of the Ballistic Research Laboratories for cooperation in providing self-recording pressure gauges and records reduction to augment Sandia Corporation equipment and data on this experiment.

CONTENTS

ILLUSTRATIONS

ILLUSTRATIONS (Continued)

TABLES

CHAPTER 2 INSTRUMENTATION

CHAPTER 3 RESULTS

CHAPTER 1

INTRODUCTION

1.1 OBJECTIVE

The objective of Project 1.3 was to measure at an array of ground stations the peak ground-level overpressures, both directly incident (free air) and reflected (near the ground), resulting from the Shot 10 high-altitude detonation. Experimental results were to be used to examine free-air pressure scaling techniques, surface reflection of shocks, and the effect of atmospheric structure. Should the blast efficiency of the high-altitude detonation be appreciably lower than that obtained on low-altitude detonations, the measured incident overpressures on the ground would be a very rough index of such changes in blast efficiency.

1.2 BACKGROUND AND THEORY

A nuclear detonation is a complicated series of events in which each of the parameters such as thermal radiation and blast energy can, to a large extent, undergo mutual interactions. Although previous studies indicate that there is probably only a small change in the blast efficiency over the first 40,000 ft of atmosphere,[1] the studies were qualified with statements that several details of a detonation at 40,000 ft could not be determined very accurately.

The general trend was a decrease of blast efficiency with altitude. However, Project 1.3 results are not particularly valuable as a check on yield; that is, when the shock wave reaches ground stations it has traveled a considerable length through an inhomogeneous atmosphere. Therefore Sachs' or modified Sachs' scaling cannot be used, with complete confidence, to scale results for comparison with the free-air pressure curve. Project 1.3 results are accordingly valuable as a check on scaling laws, providing the yield, blast efficiency, and free-air pressure curve (for a homogeneous atmosphere) are known.

Sachs' scaling[2] of shock parameters from a given burst in one homogeneous atmosphere is used to predict the parameters to be experienced from a different yield in a different homogeneous atmosphere. Thus, when

$$\Delta P_1 = \Delta P_0 \left(\frac{P_1}{P_0}\right) \tag{1.1}$$

then, with a given burst of 1 kt,

$$\begin{aligned} R_1 &= R_0 \left(\frac{P_0 W_1}{P_1 W_0}\right) \\ &= R_0 \left(\frac{P_0 W_1}{P_1}\right)^{1/3} \end{aligned} \tag{1.2}$$

and

$$t_1 = t_0 \left(\frac{P_0 W_1}{P_1 W_0}\right)^{1/3} \left(\frac{T_0}{T_1}\right)^{1/2}$$
$$= t_0 \left(\frac{P_0 W_1}{P_1}\right)^{1/3} \left(\frac{T_0}{T_1}\right)^{1/2} \tag{1.3}$$

where ΔP = overpressure
P = atmospheric pressure
R = slant range
W = kiloton yield
t = time
T = absolute temperature
Subscripts 0,1 refer to the given burst and predicted burst parameters, respectively.

This prediction process is often used to obtain effects expected after passage of a blast wave through a nonhomogeneous atmosphere; i.e., to a gauge situated at a different altitude from the burst.[3] This method, "A-scaling,"[4] is usually called Sachs' scaling. It states that when

$$\Delta P_0 = \Delta P_G \left(\frac{P_0}{P_B}\right) \tag{1.4}$$

then, to scale to a 1-kt burst at sea level,

$$R_0 = R_G \left(\frac{P_B}{P_0 W_B}\right)^{1/3} \tag{1.5}$$

and

$$t_0 = t_B \left(\frac{P_B}{P_0 W_B}\right)^{1/3} \left(\frac{T_B}{T_0}\right)^{1/2} \tag{1.6}$$

where subscripts 0,G,B = sea level, gauge, and burst conditions, respectively.

Modified Sachs' scaling was proposed[5] to improve prediction of overpressures when gauge conditions differed from burst conditions. Use of modified Sachs' scaling indicates that shock parameters depend on the ambient conditions at the gauge. Here, when

$$\Delta P_0 = \Delta P_G \left(\frac{P_0}{P_G}\right) \tag{1.7}$$

then, to scale to 1 kt at sea level,

$$R_0 = R_G \left(\frac{P_G}{P_0 W_B}\right)^{1/3} \tag{1.8}$$

and

$$t_0 = t_G \left(\frac{P_G}{P_0 W_B}\right)^{1/3} \left(\frac{T_G}{T_0}\right)^{1/2} \tag{1.9}$$

A more complex theoretical system involving corrections for nonhomogeneous atmospheric propagation paths is available,[6] and a few numerical computations have been carried out or

proposed.[7-9] These different methods give differing results which are not considered in this report.

Previous measurements on surface or low air bursts have often given smaller overpressures than would be predicted by a Kirkwood-Brinkley extension of the Tumbler-Snapper composite free-air pressure vs distance curve to low overpressures of 0.5 psi and below.[10] One factor that reduces overpressures is an upward divergence of the shock front due to higher surface temperatures and, hence, acoustic refraction. On the other hand, early morning low-level bursts at the Nevada Test Site (NTS) frequently give higher-than-predicted overpressures at the low overpressures. This is usually caused by refractive ducting under a surface temperature inversion; Teapot Shot 4 damage to the Federal Civil Defense Administration structures at 7 miles is an example of this effect.[11] No precise quantitative analyses of these pressure variations have been successful because surface terrain and atmospheric inhomogeneities interfere with the systematic collection of impulses from the number of possible ray paths of travel.[12]

Shot 10 gave fractional pounds-per-square-inch overpressures at relatively short ground range without complications, due to interactions between the terrain and the surface air layer. A single ray-travel path exists to each observation point for nearly 30 miles ground range. A relatively small correction for refractive divergence, differing from spherical expansion, may be computed from the atmospheric conditions using sound ray-path techniques.[10,12] Any further deviations from the scaled pressure-distance curve extrapolation, if they occur, must be explained by other than refraction effects.

Blast-wave asymmetry is of interest in predicting overpressures in nonhomogeneous atmospheres at levels different from burst altitude. A check observation of overpressures and arrival times at points near and circling Ground Zero provides data on the shape of the wave front. With the acoustic assumption, the shape may be computed from the atmospheric conditions of wind and temperature; a comparison with the observed shape shows the relative significance of sound velocity and pressure-altitude gradients as sources of distorted effects.

In addition to providing information about spherical shock distortion, this study was also useful for long-range damage prediction. To predict pressure amplitudes at great distances, where atmospheric ducting is present, a knowledge of the energy reflection efficiency for bounces of the signal from the ground is necessary.[12] A theoretical reflection factor for topsoil in the frequency range involved may be computed to be 0.997 by assuming acoustic coupling across the density discontinuity to the ground surface.[13] This value seems too high when compared with statistical interpretations from observations. Shot 10 provided a shock wave approaching the ground at a high-incidence angle even in the acoustic pressure region. Instruments mounted on poles were used to detect separately the overpressure of both the incident pressure and reflected signals. In this way the reflection factor (i.e., reflected energy divided by incident energy) was obtained, since the wave shape and time parameters of the two components may be assumed to be the same in integrating:

$$E = \int_t \frac{(\Delta P)^2 \, dt}{\rho V} \tag{1.10}$$

where E = energy
P = peak overpressure
ρ = ambient air density
V = ambient wave velocity

Thus, energy is proportional to the square of the peak overpressure since ambient air density and ambient wave velocity are constant in the acoustic case. Several stations were set up to measure this reflection factor, giving a check on the functional dependence of reflection factor upon pressure amplitude, incidence angle, and, to a certain degree, terrain roughness.

REFERENCES

1. F. H. Shelton, Phenomenology of a High-altitude Atomic Explosion; Sandia Corporation, SC-3363(TR), Apr. 28, 1954.
2. R. G. Sachs, Dependence of Blast on Ambient Pressure and Temperature, Ballistic Research Laboratories, BRL-466, May 15, 1944.
3. H. Scoville, Jr., et al., Final Summary Report to the Test Director, Operation Tumbler-Snapper, WT-514, May 1953.
4. V. Salmon, Air Pressure Vs Time, Operation Tumbler-Snapper, WT-512, February 1953.
5. J. W. Bond, Scaling of Peak Overpressures in a Nonuniform Atmosphere, Sandia Corporation, SC-1939(TR), July 1951.
6. H. A. Bethe, Blast Wave, Los Alamos Scientific Laboratory, LA-1021, Vol. VII, Part II, August 1942.
7. F. C. Ledsham and H. H. M. Pike, The Effect of Atmospheric Variations on the Propagation of Blast Waves to High Altitudes, Armament Research Establishment, 31/50, January 1950.
8. F. Theilheimer and L. Rudlin, The Influence of Atmospheric Pressure and Temperature Variations on Shock Wave Propagation, Part I, Naval Ordnance Laboratory, NAVORD-2707, October 1953.
9. P. C. Fife, Numerical Calculation of a Blast Wave in a Nonuniform Atmosphere, Sandia Corporation, TM-253-54-51, Nov. 15, 1954.
10. C. D. Broyles, Comparison of the Modified Sachs' Scaling with Experiments, Sandia Corporation, TM-274-54-51, Dec. 14, 1954.
11. Bruce G. Johnston, Damage to Commercial and Industrial Buildings Exposed to Nuclear Effects, Operation Teapot, Project 31.2, ITR-1189, May 1955.
12. E. F. Cox et al., Damaging Air Shocks at Large Distances from Explosions, Operation Buster-Jangle, WT-303, Apr. 24, 1952.
13. E. F. Cox, Sound Propagation in Air, Sandia Corporation, TM-136-54-51, July 12, 1954.

CHAPTER 2

INSTRUMENTATION

Three types of pressure transducers were operated during Shot 10 (see Fig. 2.1 for locations).

Sandia Corporation Blast Prediction Unit operated Wiancko 3-PBM-2 microbarographs[1] at the Control Point, Camp Mercury, and at the intersection of the main area access road and

Table 2.1 — METEOROLOGICAL DATA

Altitude, 10^3 ft MSL	Wind: Direction, deg	Wind: Speed, knots	Temp., °C	Pressure, mb
Surface	030	09	+10.5	885
5	020	10	+7.0	851
6	040	15	+4.1	820
8	040	16	−2.3	760
10	030	13	−6.8	705
12	020	16	−9.5	652
14	360	16	−13.2	602
16	010	12	−18.0	554
18	010	18	−23.0	511
20	010	18	−27.3	470
25	350	18	−40.0	377
30	310	27	−47.7	301
35	320	27	−47.2	238
36.64*	300	28	−47.8	222
40	290	43	−45.9	190

* Burst altitude.

the Frenchman Flat turnoff road. All sensing units were mounted on 60-ft poles to obtain both incident free-air and reflected overpressures. By using various set ranges it was possible to measure pressure pulse amplitudes from 1 μb (1 μb = 1.5×10^{-5} psi) to 24 mb (24 mb = 0.35 psi). Records were obtained on Brush recorders at 12.5 cm/sec paper speed.

At Ground Zero and at 12,000 and 24,000 ft from Ground Zero on a line toward the Control Point, Sandia operated millibarographs.[2] These were ¼-psi Northam transducers. At the 12,000-ft station a Wiancko 1-psi transducer was used for comparison. At Ground Zero two transducers were mounted on a 32-ft pole, and two were placed at ground level. Records were obtained with a new d-c system.[3] One transducer at 24,000 ft and two at 12,000 ft were set at

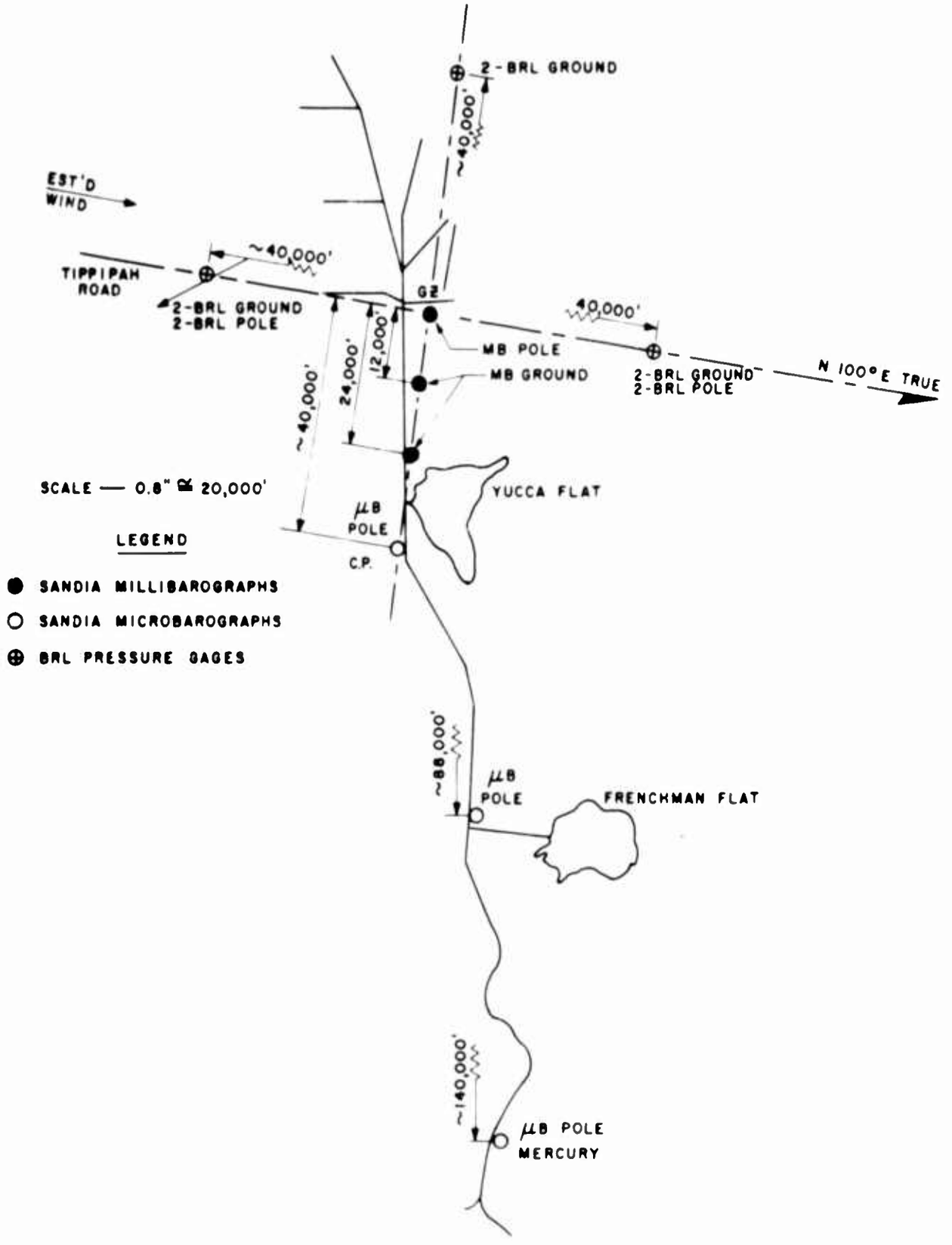

Fig. 2.1 — Shot 10 ground pressure-instrument locations.

[redacted]

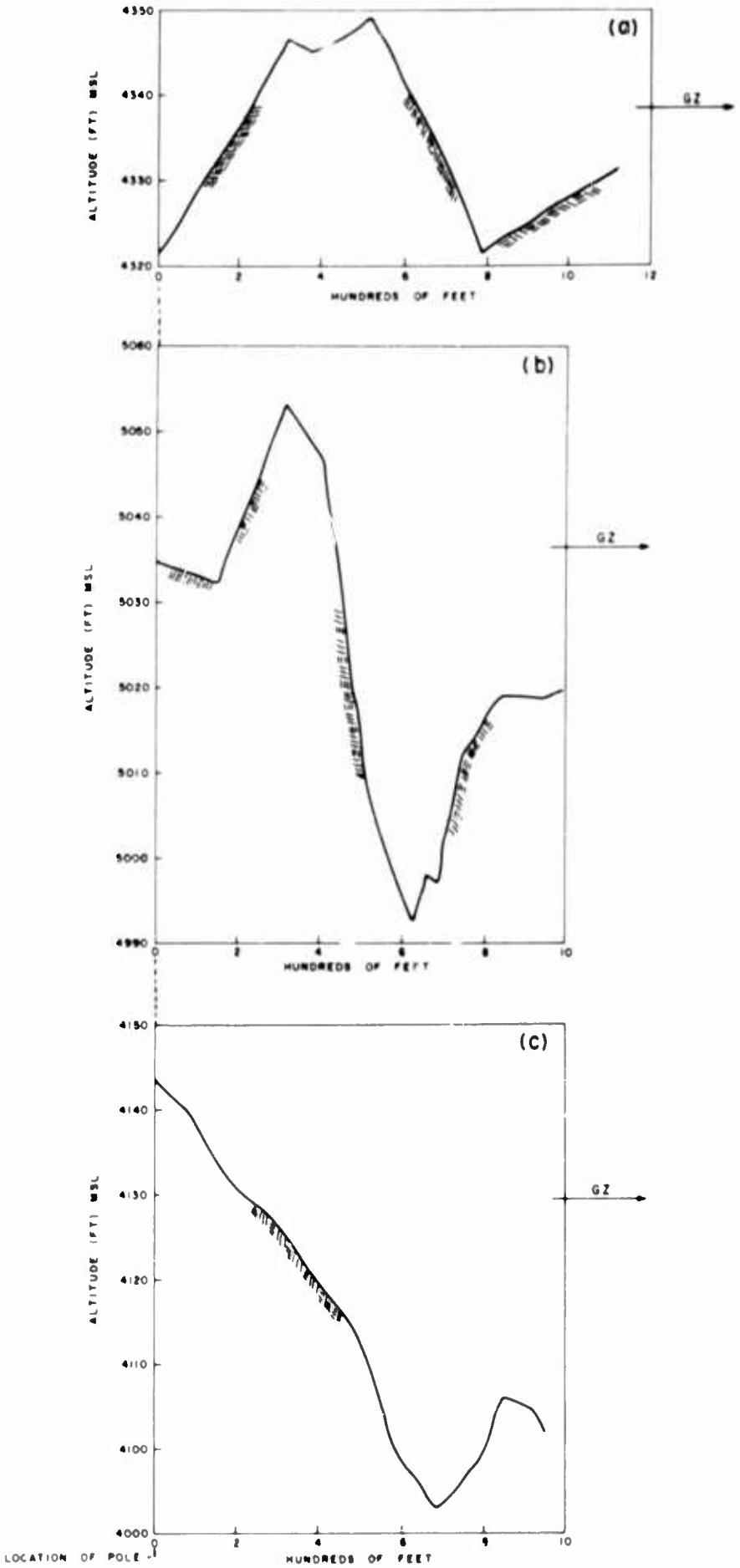

Fig. 2.2 — Ground profile to: (a) 7-mile station, east; (b) 7-mile station, west; and (c) Control Point.

ground level with recordings made by Consolidated D systems. All recorders were activated by an Edgerton, Germeshausen, and Grier (EG&G) signal, and a zero time mark was recorded from an EG&G Blue Box signal.

Ballistic Research Laboratories (BRL) provided self-recording very low pressure (VLP) microbarographs for measurements at approximately 40,000 ft from Ground Zero in the north, east, and west directions.[4] Personnel from BRL installed these recorders and reduced their records. Sensing elements were mounted at ground level and on 60-ft poles at the east and west stations but were mounted only at ground level at the north site.

All barograph unit locations were surveyed to ±1 ft. For the reflection-factor computation, a ground profile extending 1000 ft toward Ground Zero was necessary for each pole-mounted unit. Profiles toward the east and west 7-mile stations and the Control Point are shown in Fig. 2.2.

Weather data consisting of temperatures, pressures, and wind direction and speed, from surface to 93,000 ft mean sea level (MSL), were obtained from the Air Weather Service; the data at levels selected for acoustical analysis are shown in Table 2.1.

REFERENCES

1. Microbarograph Evaluation Report, Sandia Corporation, SC-2990(TR), Sept. 18, 1953.
2. G. W. Rollosson, Test Procedures and Instrumentation for Projects 1.1c, 1.1d, 1.4a, and 1.4b, Operation Upshot-Knothole, WT-787, June 1954.
3. G. W. Rollosson, Static and Dynamic Overpressure Measurements; Operation Teapot, Project 39.2, ITR-1192, May 1955.
4. J. J. Meszaros, Ground Surface Air Pressure Vs Distance from High-yield Detonations; Operation Castle, WT-905.

CHAPTER 3

RESULTS

3.1 GENERAL

Shot 10 was detonated at approximately 1000 Pacific Standard Time, 6 April 1955. Burst altitude furnished by EG&G was 36,645 ± 30 ft MSL; the actual Air Zero was 404 ± 25 ft west and 57 ± 20 ft south of intended Ground Zero. Ground Zero altitude was 4038 ft MSL; thus the burst height above ground was 32,607 ± 30 ft. By radiochemical analysis the yield of the weapon was found to be 3.3 ± 0.4 kt.

Table 3.1 — STATION LOCATIONS AND SLANT RANGES

Station	Elevation, ft MSL	Ground range, ft	True heading, burst-to-gauge, deg	Slant range, ft	Pole height, ft
Ground Zero	4,038	408	82.0	32,610	34
12,000 ft south of Ground Zero	3,969	11,979	177.7	34,732	
24,000 ft south of Ground Zero	3,990	23,943	178.7	40,492	
Control Point	4,144	34,158	177.5	47,149	60
Frenchman Flat turnoff	3,229	82,072	169.7	88,614	60
Mercury Quonset No. 28	3,795	135,804	171.4	139,721	60
7 miles east of Ground Zero	4,330	37,309	100.2	49,358	60
7 miles west of Ground Zero (not surveyed)	4,960	39,560	279.6	50,750	58
7 miles north of Ground Zero	4,250	36,008	0.3	49,183	
Air Zero	36,645				

Ground ranges and slant ranges of the various stations are listed in Table 3.1. Arrival times and initial overpressures are given in Table 3.2; Fig. 3.1 defines these quantities. Ground-surface pressures from pole measurements were calculated by taking the sum of two pressure steps, P_2 and $(P_4 - P_3)$. A probable error of 5.2 per cent for these readings may be derived by examining the internal consistency of the measurements at Ground Zero. However, this includes a reading based on faulty calibration, and, if it is ignored, the probable error is

Table 3.2 — INITIAL OVERPRESSURES AND ARRIVAL TIMES FOR SHOT 10

Gauge No.	Station	Gauge type	Overpressures P_1, psi	P_2, psi	P_3, psi	P_4, psi	Arrival times T_1, sec	T_2, sec	T_3, sec	T_4, sec	Remarks
1	Ground Zero*	Northam	0.150				30.060		31.118	33.840	
2	Ground Zero*	Northam	0.199				30.060		31.113	33.820	Faulty calibration
3	Ground Zero*	Northam	0.139	0.072	0.067	0.134	30.030	30.092	31.133	33.960	
4	Ground Zero†	Northam	0.124	0.065	0.057	0.116	30.030	30.091	30.660	32.710	Faulty leak plug
5	12,000 ft* south of Ground Zero	Northam	0.160				33.228		34.348	37.130	E 0.168‡ (shows pressure hump at about 90 msec after initial peak)
6	12,000 ft* south of Ground Zero	Wiancko	0.156				33.228		34.640	37.950	E 0.172‡
7	24,000 ft* south of Ground Zero	Northam	0.085				39.1		40.2	43.1	E 0.118‡ (shows pressure hump at about 70 msec after initial peak; front shows some rounding)
8	40,000 ft† east of Ground Zero	BRL	0.112	0.059	0.045	0.098	46.1	46.161	47.256	49.728	
9	40,000 ft† east of Ground Zero	BRL				0.095					Did not run; peak pressure only
10	40,000 ft* east of Ground Zero	BRL	0.099				45.9		46.875	49.397	

11	40,000 ft* east of Ground Zero	BRL	0.106				46.2		47.585	50.275	
12	40,000 ft† west of Ground Zero	BRL	0.087	0.045	0.043	0.085	47.8	47.884	49.154	51.210	
13	40,000 ft† west of Ground Zero	BRL	0.101	0.045	0.039	0.095	48.2	48.283	49.645	51.791	
14	40,000 ft* west of Ground Zero	BRL	0.089				44.8		45.651	47.401	Never got up to speed
15	40,000 ft* west of Ground Zero	BRL	0.075				47.9		49.215	51.638	Extradamped
16	40,000 ft* north of Ground Zero	BRL	0.100								Did not run; peak pressure only
17	40,000 ft* north of Ground Zero	BRL	0.093								Did not run; peak pressure only
18	Control Point†	Microbarograph	0.115	0.060	0.061	0.116	43.13	43.20	44.22	46.55	
19	Frenchman Flat†	Microbarograph	0.073				83.12		84.33	86.92	No step
20	Mercury†	Microbarograph	0.018				127.98		129.28	131.62	Weak step not readable

* Ground station.

† Pole station.

‡ Shows pressure hump about 100 msec after initial peak; estimated peak extrapolated forward from hump shown in remarks.

reduced to below 1 per cent. For caution, a limit of 10 per cent error is assigned to the 12,000- and 24,000-ft stations since no electronic gain correction was employed at these stations; sensitivity shifts up to 10 per cent have been observed with the equipment employed. The microbarographs usually have an error of less than 5 per cent; however, they have a response time of about 10 msec.

Two Ground Zero pressure-time records are displayed in Figs. 3.2 and 3.3. Figures 3.4 and 3.5 show records from the 12,000- and 24,000-ft stations, respectively, which do not show the classical wave shape of exponential decay but show instead a typical peak and decay followed by a pressure hump. In Fig. 3.5 the hump pressure exceeds the initial pressure if the wave-front gauge ringing is discounted. This phenomenon is real but is not understood. Similar wave shapes noted in microbarograph observations from low bursts under inversions have been explained as interference phenomena.

However, in Shot 10 no interference or multiple ray paths seem possible. A mechanism for a delayed secondary impulse is reflection from a temperature-discontinuity surface which might exist near the ground, remaining from the usual nighttime inversion. Indeed, the delay of the hump behind the shock front suggests such a layer at about the same height above ground over the 12,000- and 24,000-ft stations. However, at the incidence angle involved, less than ½ per cent of the reflected wave energy would be reflected from a 10°C inversion. This is an order of magnitude too low to account for the secondary pulse observed. It also seems unlikely that a pulse results from interaction with the surface since the angle between the incident shock and the ground is small. The obvious possibilities left are that the phenomenon represents: a shock-wave decay stage; an unexpected secondary pulse within the sphere of shocked air which is the result, perhaps, of the large-scale inhomogeneity; or an absorption of high-frequency components near the shock front in the reflection. Examples of records obtained by BRL are shown in Fig. 3.6. Although ringing is evident in the records, reasonably accurate (±15 per cent) estimates of initial pressure may be made from the traces. These also show a pressure hump, but the effect is not nearly so pronounced as at the 12,000- and 24,000-ft stations.

The incident overpressures as a function of slant range, scaled to 1 kt, free air, and mean sea level, have been plotted in Fig. 3.7. A pressure reflection factor of 0.92, obtained as the average of the reasonable values in Table 3.5, was used to obtain incident free-air pressure at stations where only ground pressure measurements were made. Results are tabulated in Table 3.3. For comparison, the pressure-distance curves from reference 1 (to 0.10 psi) and reference 2 (to 0.07 psi) are shown extended by the semiacoustic theory.[3] These curves have been selected for this comparison as the most recent and reliable. It will be noticed that scaled, measured overpressures lie slightly below those predicted by the extrapolated reference curves when modified Sachs' scaling is used but are quite high when the usual scaling is employed. It thus seems that modified Sachs' scaling is more appropriate. However, the experiment is not completely definitive since the true free-air pressure curve has not been determined in this pressure region.

3.2 TIME-OF-ARRIVAL SCALING

Table 3.4 shows a comparison of observed shock arrival times at various stations with the sound arrival times computed for the slant range and integrated through the observed atmospheric conditions of temperature and winds. It appears that the Ground Zero, Control Point, and 7-mile stations had accurate time bases, whereas the other clocks were fast. An approximate correction necessary to bring the observed times from the fast clocks up to the apparently correct clocks' average differences is included in the table. The Sachs'-scaled arrival time should differ from acoustic arrival time at ambient 222-mb pressure and −47°C by 1.75 sec; but, since the ambient pressure is increasing along the downward-directed shock ray, the observed difference should be smaller, and 1.7 sec seems reasonable. On the other hand, an arrival difference of 0.98 sec is obtained by modified Sachs' scaling.

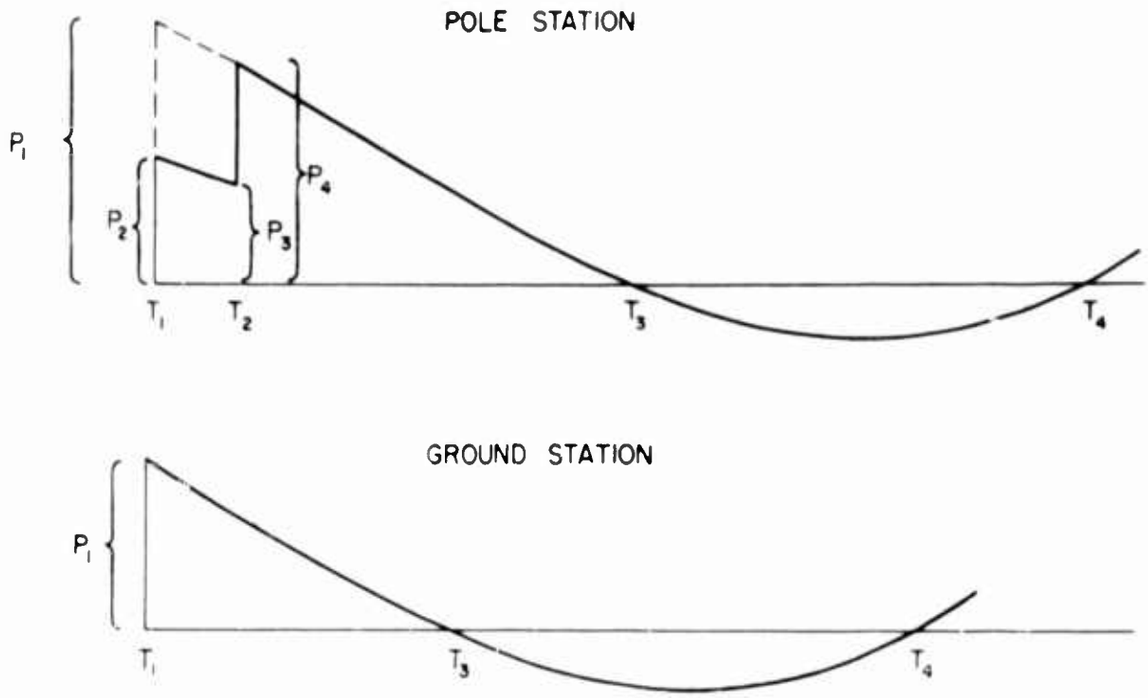

Fig. 3.1 — Definitions of times of arrival and overpressures on typical wave forms.

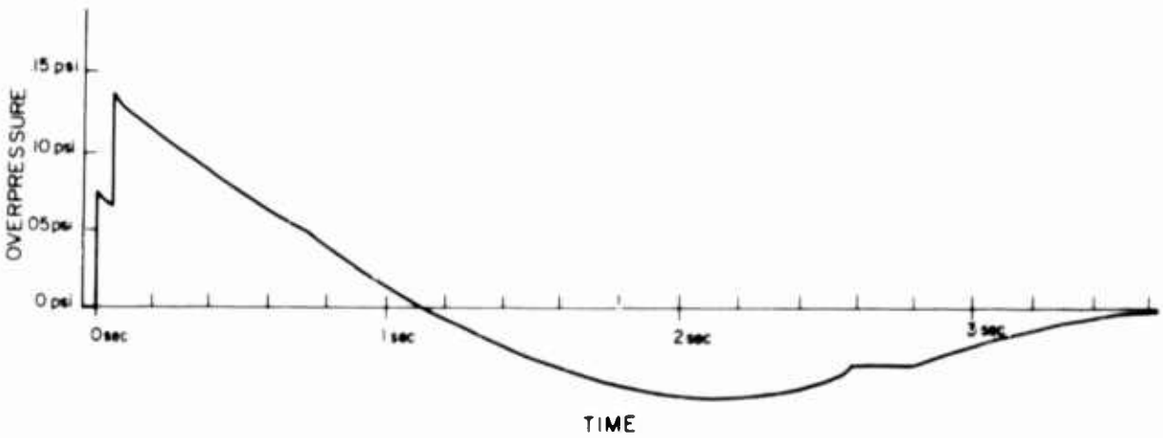

Fig. 3.2 — Pressure-time record taken at Ground Zero (pole).

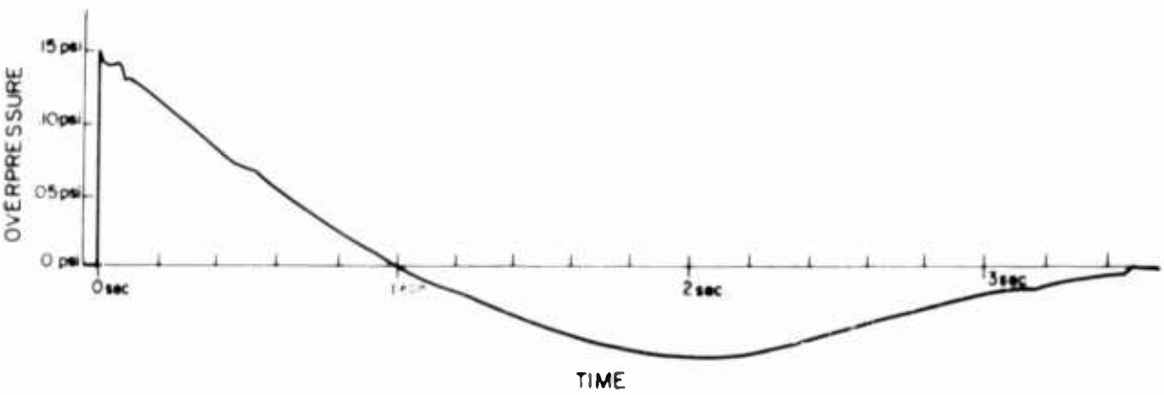

Fig. 3.3 — Pressure-time record taken at Ground Zero (ground).

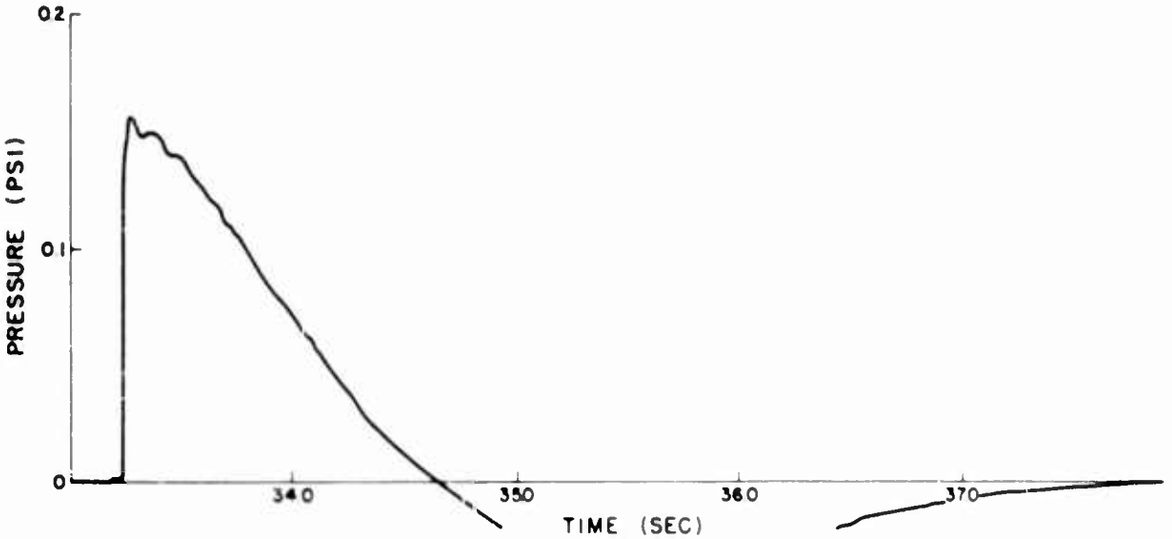

Fig. 3.4 — Pressure-time record taken at 12,000-ft station.

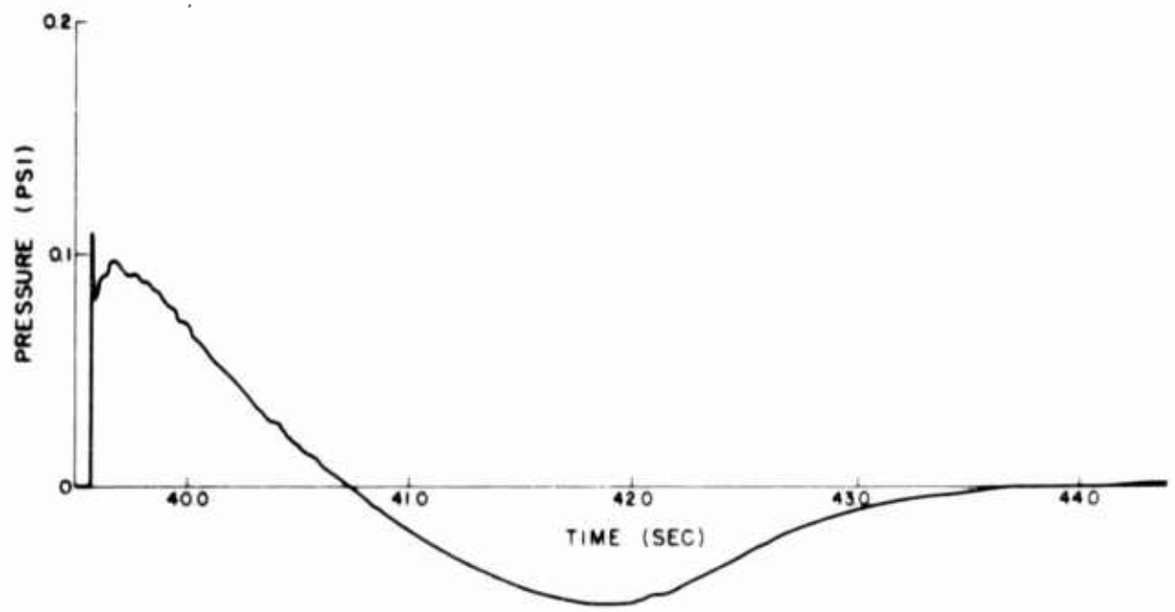

Fig. 3.5 — Pressure-time record taken at 24,000-ft station.

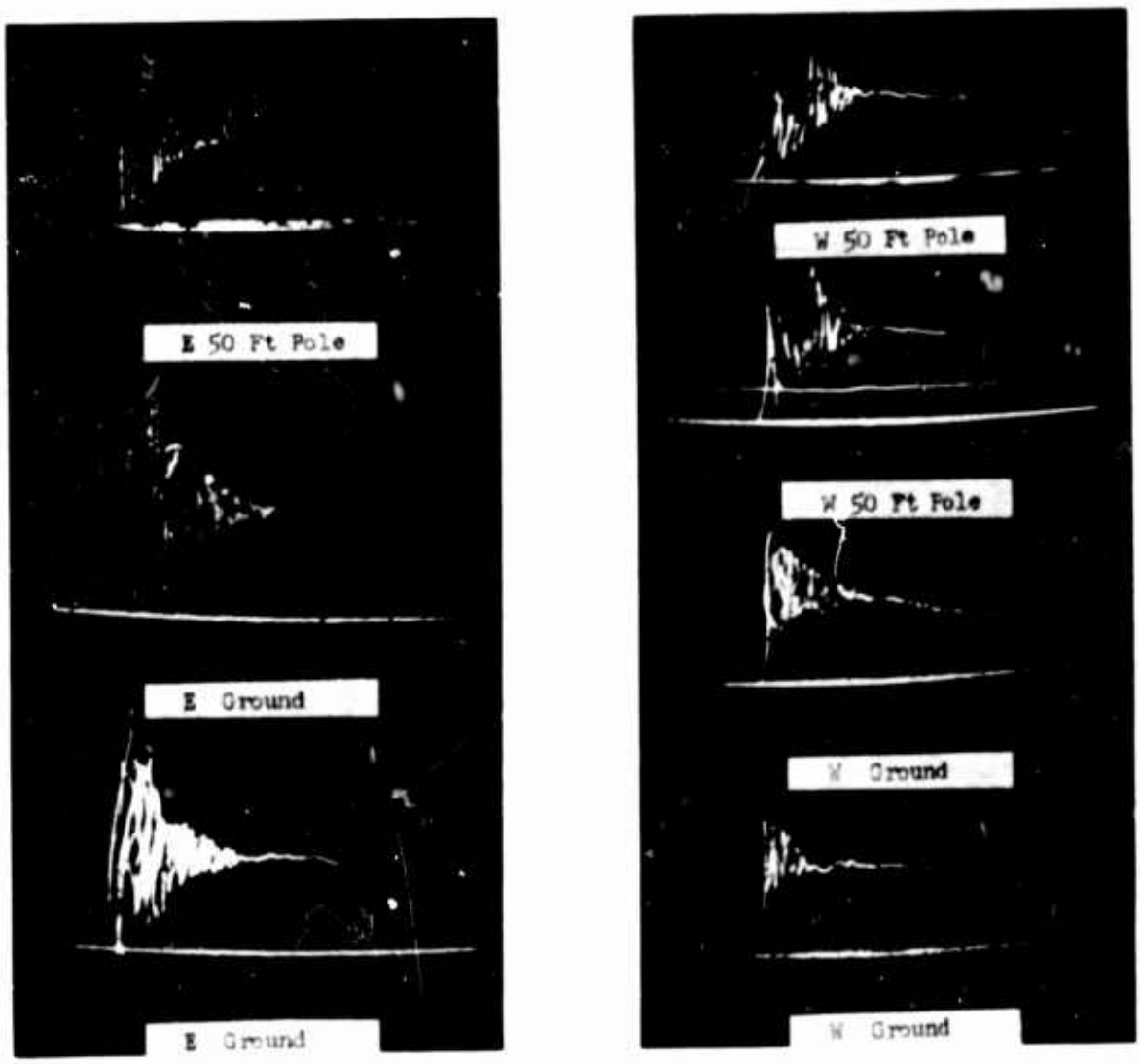

Fig. 3.6 — Examples of BRL overpressure records, Shot 10, 40,000-ft stations east and west.

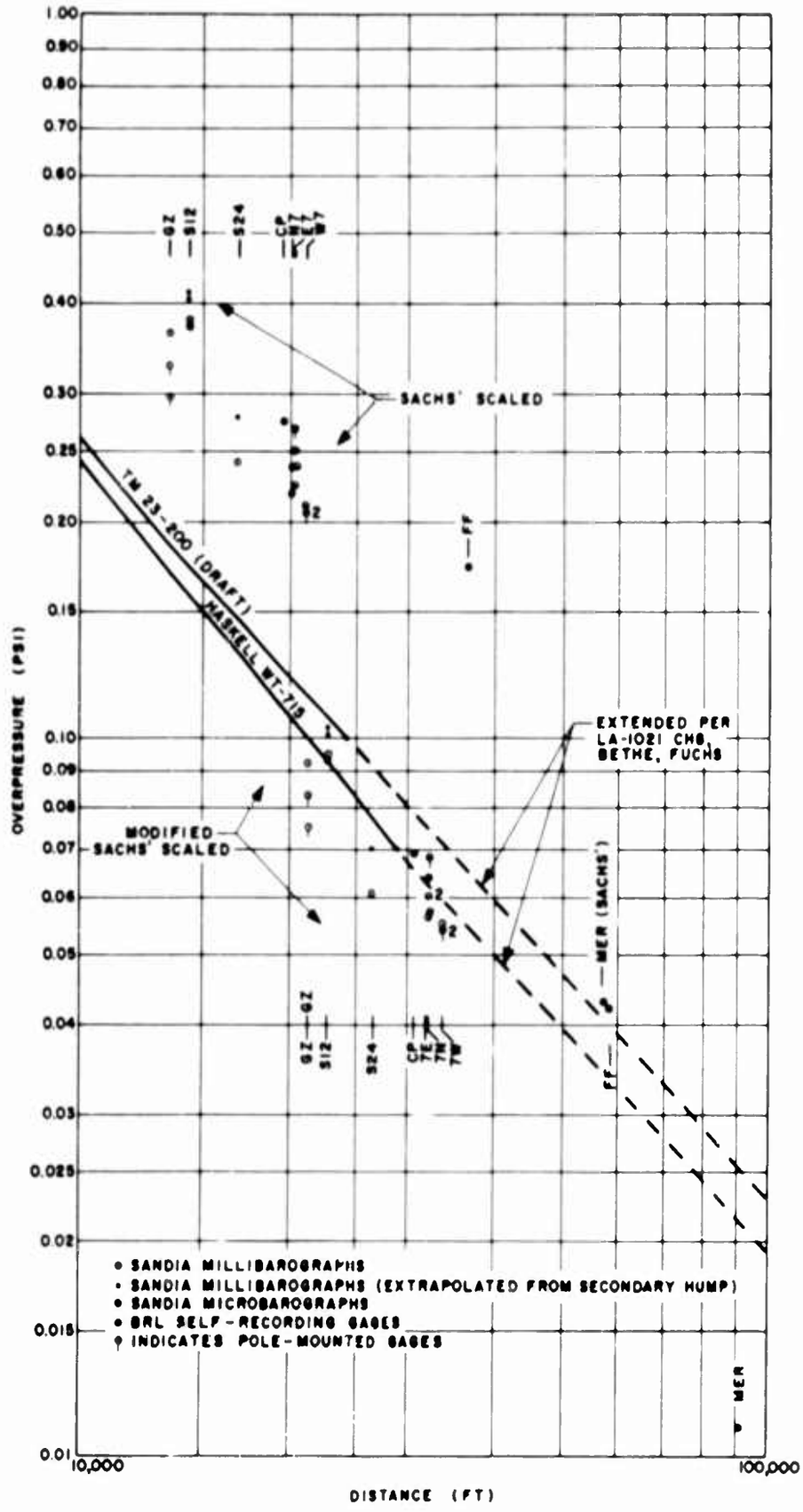

Fig. 3.7 — Incident pressures vs slant range (scaled to 1 kt, free air, mean sea level, by two methods).

Table 3.3—INCIDENT FREE-AIR OVERPRESSURE $P_i = P_r/1.92$

Gauge No.*	Incident overpressure, psi	Ambient pressure, mb	Modified Sachs' scaling: Incident overpressure, psi	Modified Sachs' scaling: Distance, ft	Sachs' scaling: Incident overpressure, psi	Sachs' scaling: Distance, ft
1	0.080	883	0.092	21,360	0.365	13,501
2†						
3	0.072	883	0.083	21,360	0.329	13,501
4	0.065	883	0.075	21,360	0.297	13,501
5	0.083	885	0.095	22,824	0.379	14,404
5‡	0.088		0.101		0.402	
6	0.081	885	0.093	22,824	0.370	14,404
6‡	0.090		0.103		0.411	
7	0.053	884	0.061	26,563	0.242	16,764
7‡	0.061		0.070		0.278	
8	0.059	873	0.068	32,231	0.269	20,434
9	0.049	873	0.057	32,231	0.224	20,434
10	0.052	873	0.060	32,231	0.237	20,434
11	0.055	873	0.064	32,231	0.251	20,434
12	0.045	852	0.054	32,886	0.205	21,011
13	0.045	852	0.054	32,886	0.205	21,011
14	0.046	852	0.055	32,886	0.210	21,011
15	Extradamped					
16	0.052	875	0.060	32,166	0.273	20,362
17	0.048	875	0.056	32,166	0.219	20,362
18	0.060	879	0.069	30,883	0.274	19,520
19	0.038	910	0.042	58,662	0.173	36,686
20	0.0094	891	0.011	91,797	0.043	57,844

*Gauge locations are given in Table 3.2.

†Faulty calibration.

‡Indicates values extrapolated forward from the secondary pressure hump.

Table 3.4—SIGNAL ARRIVAL TIMES

Station	Observed shock arrival time, sec	Computed sound arrival time, sec	Difference (sound−shock), sec	Time correction factor
Ground Zero	30.060	31.734	1.674	
12,000 ft south of Ground Zero	33.228	33.418	0.190	0.95507
24,000 ft south of Ground Zero	39.367	38.676	−0.941	0.93495
Control Point	43.130	44.829	1.699	
Frenchman Flat turnoff	83.120	83.695	0.575	0.98667
7 miles east of Ground Zero	46.050	47.438	1.388	0.99359
7 miles west of Ground Zero	47.900	49.577	1.677	

3.3 NEGATIVE-PHASE-DURATION SCALING

Since the incident pressure wave is nearly acoustical, durations measured at the surface may be considered identical with those in free air. At Ground Zero the observed negative-phase duration was 2.72 sec; duration corrected by factors in Table 3.4 is 2.66 sec at the 12,000-ft station and 2.83 sec at the 24,000-ft station. The average was 2.74 sec. Scaling the negative-phase duration of IBM Problem M (reference 4) to burst conditions by Sachs' scaling gives 2.77 sec for the anticipated duration. On the other hand, modified Sachs' scaling for negative-phase duration gives 1.56 sec. It is apparent that Sachs' scaling is the more proper for predicting negative-phase durations. This seems reasonable for, as pointed out in reference 5, the negative-phase duration is stabilized in the burst vicinity. Negative-phase durations used in this method of yield determination* should be Sachs'-scaled from burst conditions to sea level and 20°C.

3.4 POSITIVE-PHASE-DURATION SCALING

The positive-phase duration at Ground Zero measured approximately 1.06 sec; this value Sachs'-scaled to sea level for 1 kt gives 0.383 sec, and modified Sachs' scaling gives 0.679 sec. When pressure records observed by the Air Force Cambridge Research Center canister gauges (reference 6) at or near burst altitude are Sachs'-scaled, they show positive-phase durations which approach 0.4 sec at comparable shock strengths. The maximum duration computed in IBM Problem M scales to about 0.40 sec for 1 kt at sea level. Thus it appears that positive-phase duration is dependent upon ambient conditions at burst altitude rather than at gauge altitude for small weapons.

3.5 GROUND REFLECTION

Pressure and energy reflection factors as well as terrain characteristics are listed in Table 3.5. The pressure reflection factor is here defined as the ratio of reflected to incident overpressure $(P_4 - P_3)/P_2$ from Fig. 3.1. The energy reflection factor is defined as the square of the pressure reflection factor. This procedure is used because the energy of the wave is proportional to the square of pressure in the acoustic case. There seem to be no significant variations in the reflection factor attributable to the terrain differences.

3.6 ACOUSTICAL DISTORTION

To examine the effect of atmospheric structure, preliminary acoustic paths were computed. It was noticed that, for stations beyond the Control Point, the acoustic path was bent to nearly parallel with the surface. This accounts for the difficulty in separating incident and reflected waves at these more distant stations. Furthermore, it was found that little or no signal would be expected at Camp Mercury. Consequently, the deviation of this point on the free-air pressure curve is not surprising. The expected deviation of the observed-to-ideal (no wind or temperature gradient) overpressure for the other southern stations is given in Table 3.6.

Since these aberrations are smaller than probable error, no correction for this effect has been employed in the free-air pressure data (Fig. 3.7). Also, acoustical distortion would affect the arrival times by amounts smaller than the timing errors encountered; thus the validity of acoustic distortion theories cannot be verified with the results of this experiment. The Raypac (reference 7) plot for acoustic propagation to the south is shown in Fig. 3.8.

---

* This method relates radiochemical yield (W) and negative-phase duration (θ) by the expression $W = K(\theta)^3$. The coefficient K is 0.5 kt/sec^3 for a low burst which forms a Mach stem and 1.0 kt/sec^3 for a high burst. Results of Shot 1C are in agreement with this equation.

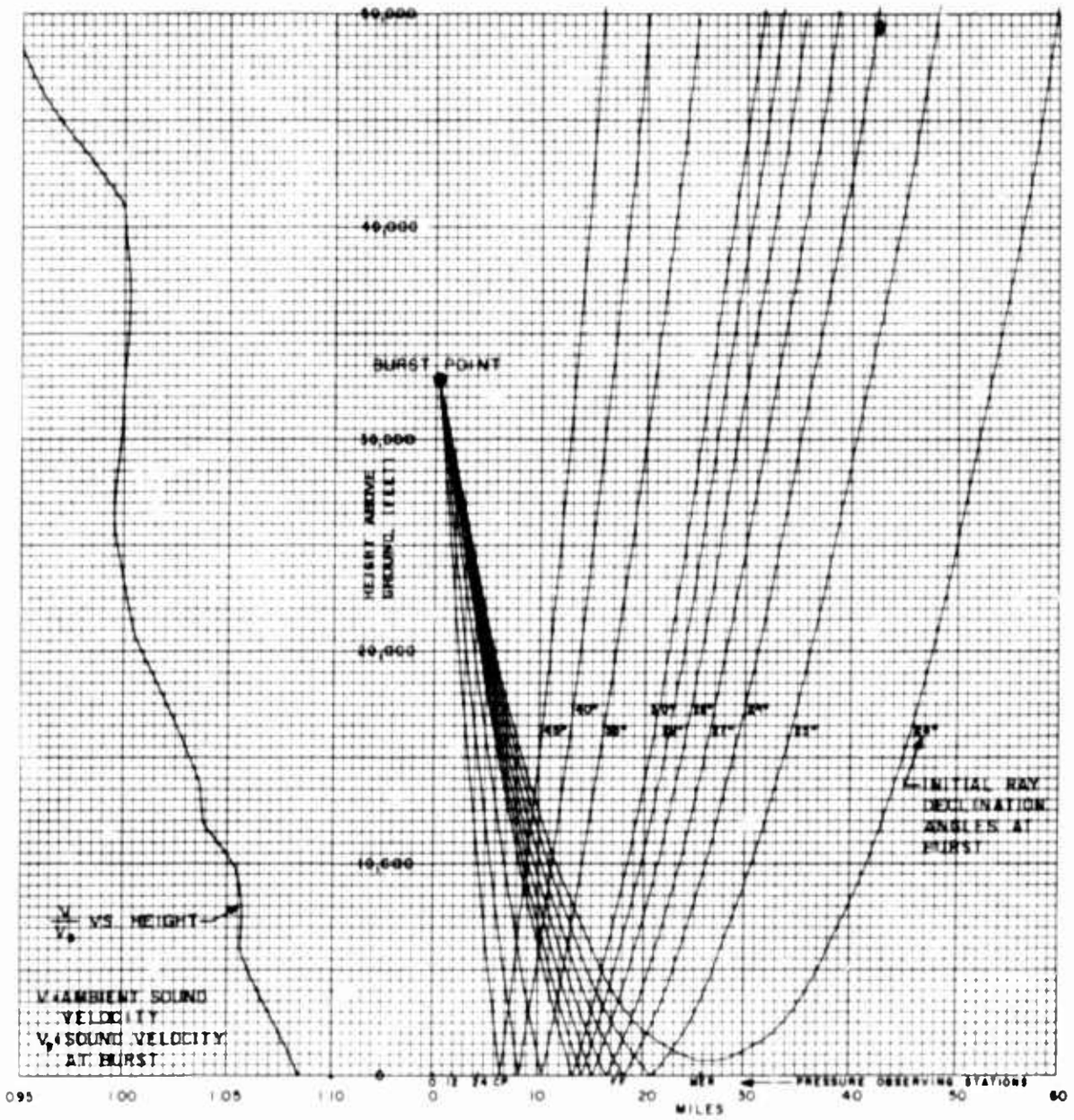

Fig. 3.8 — Raypac plot for acoustic propagation to the south of burst zero, Shot 10.

Table 3.5 — PRESSURE AND ENERGY REFLECTION FACTORS

Station	Pressure reflection factor	Energy reflection factor	Terrain features
Ground Zero	0.930	0.863	Flat with brush
Ground Zero	0.908	0.824	Flat with brush
7 miles east of Ground Zero	0.900	0.810	30 ft toward Ground Zero, rocky
7 miles west of Ground Zero	0.940	0.882	20-ft hill; 40-ft dip toward Ground Zero; rocky
7 miles west of Ground Zero	1.240	1.536	(Doubtful record; not included in averages)
Control Point	0.920	0.845	50-ft downward slope toward Ground Zero; rocky
Average	0.9196	0.8448	
Standard deviatio	±0.0145	0.0259	

Table 3.6 — EXPECTED DEVIATION OF OVERPRESSURES CAUSED BY TEMPERATURE GRADIENTS AND WINDS

Station	Expected ratio of observed pressure to ideal pressure
Ground Zero	1.000
12,000 ft south of Ground Zero	0.956
24,000 ft south of Ground Zero	0.986
Control Point	0.974
Frenchman Flat turnoff	1.028

REFERENCES

1. Capabilities of Atomic Weapons (Draft Copy), AFSWP, Revised Dec. 1, 1954.
2. N. A. Haskell and Maj R. M. Brubaker, Free Air Atomic Blast Pressure Measurements; Operation Upshot-Knothole, Project 1.3, Report WT-715, April 1954.
3. H. A. Bethe and K. Fuchs, Asymptotic Theory for Small Blast Pressure, LASL Report LA-1021, Chap. 8, p. 46, Aug. 12, 1947.
4. IBM Problem M (performed at Los Alamos Scientific Laboratory), original data tabulations.
5. M. Cowan, Negative-phase Duration as a Measure of Blast Yield, Sandia Corporation, SC-3170(TR), Sept. 1, 1953.
6. N. A. Haskell et al., Measurement of Free Air Atomic Blast Pressures; Project 1.1, Operation Teapot, WT-1101.
7. H. B. Durham, Raypac — A Special-purpose Analog Computer, Sandia Corporation, TM-46-55-54, Mar. 24, 1955.

CHAPTER 4

CONCLUSIONS AND RECOMMENDATIONS

4.1 CONCLUSIONS

Shock overpressures at surface levels from high-altitude bursts may be more accurately predicted with modified Sachs' scaling than with ordinary Sachs' scaling. Modified Sachs'-scaled observations showed about 20 per cent lower overpressures than those expected from the free-air pressure-distance curve, whereas ordinary Sachs'-scaled observations measured about twice the expected overpressures. Similarly, predictions made by modified Sachs' scaling of the extended overpressure curve give results slightly higher than observed.

Positive- and negative-phase durations and the difference between acoustic and shock arrival times were found to satisfy ordinary Sachs' scaling. Thus the time parameters for small-yield weapons depend upon ambient conditions at burst altitude and the strong shock region, and not upon conditions at or near the observing point.

Measurement of the surface-pressure reflection coefficient was not as definitive as had been hoped for, but an average value of 0.92 was confirmed. No correlation with surface texture or incidence angle was possible. Atmospheric acoustic effects on the overpressure distribution were too small to be measured in this experiment.

4.2 RECOMMENDATIONS

If further high-altitude bursts are made, measurements should be repeated as a check on the results presented here and to further explore the effect of changes of yield, burst height, and atmospheric structure. Preliminary effort to reduce ringing characteristics of gauges would be necessary, as would use of more consistent time bases to better define the reflection factor and the acoustic distortion effect. It appears that further data from pole-mounted stations are needed to isolate the causes and to help explain the anomalous secondary pressure hump observed on some records of this experiment.

DISTRIBUTION

Military Distribution Category 5-21

ARMY ACTIVITIES

Asst. Dep. Chief of Staff for Military Operations, D/A, Washington 25, D. C. ATTN: Asst. Executive (R&SW)	1
Chief of Research and Development, D/A, Washington 25, D. C. ATTN: Special Weapons and Air Defense Division	2
Chief of Ordnance, D/A, Washington 25, D. C. ATTN: ORDTX-AR	3
Chief Signal Officer, D/A, P&O Division, Washington 25, D. C. ATTN: SIGOP	4–6
The Surgeon General, D/A, Washington 25, D. C. ATTN: Chief, R&D Division	7
Chief Chemical Officer, D/A, Washington 25, D. C.	8–9
The Quartermaster General, D/A, Washington 25, D. C. ATTN: Research and Development Div.	10
Chief of Engineers, D/A, Washington 25, D. C. ATTN: ENGNB	11–15
Chief of Transportation, Military Planning and Intelligence Div., Washington 25, D. C.	16
Commanding General, Continental Army Command, Ft. Monroe, Va.	17–19
President, Board #1, Headquarters, Continental Army Command, Ft. Sill, Okla.	20
President, Board #2, Headquarters, Continental Army Command, Ft. Knox, Ky.	21
President, Board #3, Headquarters, Continental Army Command, Ft. Benning, Ga.	22
President, Board #4, Headquarters, Continental Army Command, Ft. Bliss, Tex.	23
Commanding General, U. S. Army Caribbean, Ft. Amador, C. Z. ATTN: Cml. Off.	24
Commander-in-Chief, Far East Command, APO 500, San Francisco, Calif. ATTN: ACofS, J-3	25–26
Commanding General, U. S. Army Europe, APO 403, New York, N. Y. ATTN: OPOT Div., Combat Dev. Br.	27–28
Commandant, Command and General Staff College, Ft. Leavenworth, Kans. ATTN: ALLLS(AS)	29–30
Commandant, The Artillery and Guided Missile School, Ft. Sill, Okla.	31
Secretary, The Antiaircraft Artillery and Guided Missile School, Ft. Bliss, Tex. ATTN: Maj George L. Alexander, Dept. of Tactics and Combined Arms	32
Commanding General, Army Medical Service School, Brooke Army Medical Center, Ft. Sam Houston, Tex.	33
Director, Special Weapons Development Office, Headquarters, CONARC, Ft. Bliss, Tex. ATTN: Capt. T. E. Skinner	34
Commandant, Walter Reed Army Institute of Research, Walter Reed Army Medical Center, Washington 25, D. C.	35
Superintendent, U. S. Military Academy, West Point, N. Y. ATTN: Prof. of Ordnance	36
Commandant, Chemical Corps School, Chemical Corps Training Command, Ft. McClellan, Ala.	37
Commanding General, Research and Engineering Command, Army Chemical Center, Md. ATTN: Deputy for RW and Non-Toxic Material	38
Commanding General, Aberdeen Proving Grounds, Md. (inner envelope). ATTN: RD Control Officer (for Director, Ballistic Research Laboratories)	39–40

Commanding General, The Engineer Center, Ft. Belvoir, Va. ATTN: Asst. Commandant, Engineer School 41-43
Commanding Officer, Engineer Research and Development Laboratory, Ft. Belvoir, Va. ATTN: Chief, Technical Intelligence Branch 44
Commanding Officer, Picatinny Arsenal, Dover, N. J. ATTN: ORDBB-TK 45
Commanding Officer, Army Medical Research Laboratory, Ft. Knox, Ky. 46
Commanding Officer, Chemical Corps Chemical and Radiological Laboratory, Army Chemical Center, Md. ATTN: Tech. Library 47-48
Commanding Officer, Transportation R&D Station, Ft. Eustis, Va. 49
Director, Technical Documents Center, Evans Signal Laboratory, Belmar, N. J. 50
Director, Waterways Experiment Station, PO Box 631, Vicksburg, Miss. ATTN: Library 51
Director, Armed Forces Institute of Pathology, Walter Reed Army Medical Center, 6825 16th Street, N.W., Washington 25, D. C. 52
Director, Operations Research Office, Johns Hopkins University, 7100 Connecticut Ave., Chevy Chase, Md., Washington 15, D. C. 53
Commanding General, Quartermaster Research and Development Command, Quartermaster Research and Development Center, Natick, Mass. ATTN: CBR Liaison Officer 54-55

NAVY ACTIVITIES

Chief of Naval Operations, D/N, Washington 25, D. C. ATTN: OP-36 56-57
Chief of Naval Operations, D/N, Washington 25, D. C. ATTN: OP-03EG 58
Director of Naval Intelligence, D/N, Washington 25, D. C. ATTN: OP-922V 59
Chief, Bureau of Medicine and Surgery, D/N, Washington 25, D. C. ATTN: Special Weapons Defense Div. 60
Chief, Bureau of Ordnance, D/N, Washington 25, D. C. 61
Chief, Bureau of Ships, D/N, Washington 25, D. C. ATTN: Code 348 62
Chief, Bureau of Yards and Docks, D/N, Washington 25, D. C. ATTN: D-440 63
Chief, Bureau of Supplies and Accounts, D/N, Washington 25, D. C. 64
Chief, Bureau of Aeronautics, D/N, Washington 25, D. C. 65-66
Chief of Naval Research, Department of the Navy, Washington 25, D. C. ATTN: Code 811 67
Commander-in-Chief, U. S. Pacific Fleet, Fleet Post Office, San Francisco, Calif. 68
Commander-in Chief, U. S. Atlantic Fleet, U. S. Naval Base, Norfolk 11, Va. 69
Commandant, U. S. Marine Corps, Washington 25, D. C. ATTN: Code A03H 70-73
President, U. S. Naval War College, Newport, R. I. 74
Superintendent, U. S. Naval Postgraduate School, Monterey, Calif. 75
Commanding Officer, U. S. Naval Schools Command, U. S. Naval Station, Treasure Island, San Francisco, Calif. 76
Commanding Officer, U. S. Fleet Training Center, Naval Base, Norfolk 11, Va. ATTN: Special Weapons School 77
Commanding Officer, U. S. Fleet Training Center, Naval Station, San Diego 36, Calif. ATTN: (SPWP School) 78
Commanding Officer, Air Development Squadron 5, VX-5, U. S. Naval Air Station, Moffett Field, Calif. 79
Commanding Officer, U. S. Naval Damage Control Training Center, Naval Base, Philadelphia 12, Pa. ATTN: ABC Defense Course 80
Commanding Officer, U. S. Naval Unit, Chemical Corps School, Army Chemical Training Center, Ft. McClellan, Ala. 81
Commander, U. S. Naval Ordnance Laboratory, Silver Spring 19, Md. ATTN: EE 82
Commander, U. S. Naval Ordnance Laboratory, Silver Spring 19, Md. ATTN: EH 83
Commander, U. S. Naval Ordnance Laboratory, Silver Spring 19, Md. ATTN: R 84
Commander, U. S. Naval Ordnance Test Station, Inyokern, China Lake, Calif. 85
Officer-in Charge, U. S. Naval Civil Engineering Res. and Evaluation Lab., U. S. Naval Construction Battalion Center, Port Hueneme, Calif. ATTN: Code 753 86
Commanding Officer, U. S. Naval Medical Research Inst., National Naval Medical Center, Bethesda 14, Md. 87
Director, Naval Air Experimental Station, Air Material Center, U. S. Naval Base, Philadelphia, Pa. 88

Director, U. S. Naval Research Laboratory, Washington 25, D. C.
ATTN: Mrs. Katherine H. Cass — 89

Commanding Officer and Director, U. S. Navy Electronics Laboratory, San Diego 52, Calif. ATTN: Code 4223 — 90

Commanding Officer, U. S. Naval Radiological Defense Laboratory, San Francisco 24, Calif. ATTN: Technical Information Division — 91-92

Commanding Officer and Director, David W. Taylor Model Basin, Washington 7, D. C.
ATTN: Library — 93-94

Commander, U. S. Naval Air Development Center, Johnsville, Pa. — 95

AIR FORCE ACTIVITIES

Asst. for Atomic Energy, Headquarters, USAF, Washington 25, D. C. ATTN: DCS/O — 96

Director of Operations, Headquarters, USAF, Washington 25, D. C. ATTN: Operations Analysis — 97

Director of Plans, Headquarters, USAF, Washington 25, D. C. ATTN: War Plans Div. — 98

Director of Research and Development, Headquarters, USAF, Washington 25, D. C.
ATTN: Combat Components Div. — 99

Director of Intelligence, Headquarters, USAF, Washington 25, D. C. ATTN: AFOIN-IB2 — 100-101

The Surgeon General, Headquarters, USAF, Washington 25, D. C. ATTN: Bio. Def. Br., Pre. Med. Div. — 102

Deputy Chief of Staff, Intelligence Headquarters, U. S. Air Forces Europe, APO 633, New York, N. Y. ATTN: Directorate of Air Targets — 103

Commander, 497th Reconnaissance Technical Squadron (Augmented), APO 633, New York, N. Y. — 104

Commander, Far East Air Forces, APO 925, San Francisco, Calif. — 105

Commander-in-Chief, Strategic Air Command, Offutt Air Force Base, Omaha, Nebr.
ATTN: Special Weapons Branch, Inspector Div., Inspector General — 106

Commander, Tactical Air Command, Langley AFB, Va. ATTN: Documents Security Branch — 107

Commander, Air Defense Command, Ent AFB, Colo. — 108

Commander, Wright Air Development Center, Wright-Patterson AFB, Dayton, Ohio.
ATTN: WCRRN, Blast Effects Research — 109-110

Commander, Air Research and Development Command, PO Box 1395, Baltimore, Md.
ATTN: RDDN — 111

Commander, Air Proving Ground Command, Eglin AFB, Fla. ATTN: Adj./Tech. Report Branch — 112

Director, Air University Library, Maxwell AFB, Ala. — 113-114

Commander, Flying Training Air Force, Waco, Tex. ATTN: Director of Observer Training — 115-122

Commander, Crew Training Air Force, Randolph Field, Tex. ATTN: 2GTS, DCS/O — 123

Commandant, Air Force School of Aviation Medicine, Randolph AFB, Tex. — 124-125

Commander, Wright Air Development Center, Wright-Patterson AFB, Dayton, Ohio.
ATTN: WCOSI — 126-131

Commander, Air Force Cambridge Research Center, LG Hanscom Field, Bedford, Mass.
ATTN: CRQST-2 — 132-133

Commander, Air Force Special Weapons Center, Kirtland AFB, N. Mex. ATTN: Library — 134-136

Commandant, USAF Institute of Technology, Wright-Patterson AFB, Dayton, Ohio.
ATTN: Resident College — 137

Commander, Lowry AFB, Denver, Colo. ATTN: Department of Armament Training — 138

Commander, 1009th Special Weapons Squadron, Headquarters, USAF, Washington 25, D. C. — 139

The RAND Corporation, 1700 Main Street, Santa Monica, Calif. ATTN: Nuclear Energy Division — 140-141

Commander, Second Air Force, Barksdale AFB, La. ATTN: Operations Analysis Office — 142

Commander, Eighth Air Force, Westover AFB, Mass. ATTN: Operations Analysis Office — 143

Commander, Fifteenth Air Force, March AFB, Calif. ATTN: Operations Analysis Office — 144

Commander, Western Development Div. (ARDC), PO Box 262, Inglewood, Calif.
ATTN: WDSIT, Mr. R. G. Weitz — 145

OTHER DEPARTMENT OF DEFENSE ACTIVITIES

Asst. Secretary of Defense, Research and Development, D/D, Washington 25, D. C. ATTN: Tech. Library	146
U. S. Documents Officer, Office of the U. S. National Military Representative, SHAPE, APO 55, New York, N. Y.	147
Director, Weapons Systems Evaluation Group, OSD, Rm 2E1006, Pentagon, Washington 25, D. C.	148
Armed Services Explosives Safety Board, D/D, Building T-7, Gravelly Point, Washington 25, D. C.	149
Commandant, Armed Forces Staff College, Norfolk 11, Va. ATTN: Secretary	150
Commanding General, Field Command, Armed Forces Special Weapons Project, PO Box 5100, Albuquerque, N. Mex.	151–156
Commanding General, Field Command, Armed Forces Special Weapons Project, PO Box 5100, Albuquerque, N. Mex. ATTN: Technical Training Group	157–158
Chief, Armed Forces Special Weapons Project, Washington 25, D. C. ATTN: Documents Library Branch	159–167

ATOMIC ENERGY COMMISSION ACTIVITIES

U. S. Atomic Energy Commission, Classified Technical Library, 1901 Constitution Ave., Washington 25, D. C. ATTN: Mrs. J. M. O'Leary (for DMA)	168–170
Los Alamos Scientific Laboratory, Report Library, PO Box 1663, Los Alamos, N. Mex. ATTN: Helen Redman	171–172
Sandia Corporation, Classified Document Division, Sandia Base, Albuquerque, N. Mex. ATTN: Martin Lucero	173–187
University of California Radiation Laboratory, PO Box 808, Livermore, Calif. ATTN: Margaret Edlund	188–190
Weapon Data Section, Technical Information Service Extension, Oak Ridge, Tenn.	191
Technical Information Service Extension, Oak Ridge, Tenn. (surplus)	192–220

AEC, Oak Ridge, Tenn